AIAA SciTech Forum
11–15 & 19–21 January 2021, VIRTUAL EVENT
AIAA Scitech 2021 Forum

10.2514/6.2021-0990

Ultra-high bypass nacelle geometry design space exploration

Andrea Magrini*
Università Degli Studi di Padova, via Venezia 1, 35131 Padova - Italy

Denis Buosi†
Hit09 S.r.l., Piazzetta Bettiol 15, 35137 Padova - Italy

Ernesto Benini‡
Università Degli Studi di Padova, via Venezia 1, 35131 Padova - Italy

Christopher Sheaf§
Rolls-Royce plc., P.O. box 31, Derby, DE24 8BJ, United Kingdom

The design of a civil aeroengine nacelle is a complex multi-objective constrained problem, where several variables interact to determine the final aerodynamic performance during cruise and off-design operation. This paper presents a design space exploration of a ultra-high bypass ratio nacelle to study the relations between key geometric factors that affect the flow field past the external cowl. An in-house geometry parameterisation tool allowing a full control on the set of curves is employed in a series of sub-tasks. The investigations of axisymmetric isolated nacelles are conducted using a computational fluid dynamics tool, first studying the influence of global dimensions on the performance metrics, to restrict the feasible design space. A first optimisation with a lean numerical model is then performed to rapidly assess the effect of design variables locally changing the aerolines shapes and thus more finely controlling the pressure and isentropic Mach number distributions. Finally, a second optimisation-driven exploration employing a more advanced genetic algorithm is run, refining the feasible design space using a higher-fidelity computational model. The resulting features of the Pareto optimal solutions and the relationships between the nacelle drag coefficients with the geometric ratios can provide useful guidelines for the design of future compact nacelles for ultra-high bypass ratio turbofans.

I. Nomenclature

β_{TE}	=	Nacelle cowl trailing edge angle
C_d	=	Drag coefficient
L_{max}	=	Nacelle forebody length
L_{nac}	=	Nacelle cowl length
M_{iso}	=	Isentropic Mach number
$MFCR$	=	Mass Flow Capture Ratio
R_{hl}	=	Highlight radius
R_{max}	=	Nacelle cowl maximum radius
R_{TE}	=	Nacelle cowl trailing edge radius

II. Introduction

Future aeroengines for long haul aircraft will benefit from increased propulsive efficiency by adopting ultra-high bypass ratio (UHBPR) turbofan, to target the environmental requirements set by international institutions for the

*PhD candidate, Department of Industrial Engineering, Università Degli Studi di Padova, via Venezia 1, 35131 Padova - Italy
†Research Engineer, Hit09 S.r.l., Piazzetta Bettiol 15, 35137 Padova - Italy
‡Full Professor, Department of Industrial Engineering, Università Degli Studi di Padova, via Venezia 1, 35131 Padova - Italy
§Installation Aerodynamics, Rolls-Royce plc., P.O. box 31, Derby, DE24 8BJ, United Kingdom

2050 horizon [1]. Reducing the specific thrust has been long recognised, in fact, as a possible method to improve propulsive efficiency and reduce noise footprint and fuel cost [2–5]. The potential benefits of UHBPR turbofans are, however, hampered by the growth of engine size and weight and installation effects due to an enhanced sensitivity to external boundary conditions. In order to obtain a successful design, several constraints must be examined and the real performance of the integrated propulsive system must be assessed [6]. The engine nacelle design is, therefore, critical to a successful exploitation of the UHBPR advantages, being an important drag and weight source and affecting the flow field over a large portion of the wing. A fair amount of work has been devoted in the last years to the design of nacelle shapes, starting from two-dimensional axisymmetric isolated cases. Albert [7] employed three parameterisation techniques to optimise the nacelle external cowl and the intake shape for minimum peak Mach number at cruise and static run. Savelyev [8] performed axisymmetric and three-dimensional optimisation of nacelle and intake cowls and exhaust shape to minimise the thrust losses. Fang [9] executed a similar study employing a Class Shape Transformation (CST)-based parameterisation. Christie [10] presented a parametric tool for nacelle design based on intuitive-CST, that has been used in several other works and recently improved [11]. Robinson [12] discussed aspects of aero-engine nacelle drag by validating experimental data of ARA nacelle cowls. Tejero [13] performed a three-objective axisymmetric optimisation of the external cowl for minimum drag at cruise, spillage and divergence. The presence of several counteracting geometric parameters affecting the nacelle lands itself to a natural use of optimisation algorithms to find the best shapes fulfilling conflicting requirements at different operating conditions. The author presented the results for parametric variations of relevant geometric ratios describing the overall shape characteristics. It is well known, in fact, that reducing the nacelle length and thickness is beneficial to the weight and the cruise drag, but poses a more challenging off-design operation, due to the formation of stronger shocks and higher peaks of isentropic Mach number. Moreover, the operation at incidence and in presence of the wing upwash requires a certain lip nose radius, to avoid premature separation of the intake.

In addition to considerations on the nacelle drag characteristics, the external cowl shape must combine with the exhaust system requirements, which are dictated by the specific thermodynamic state resulting from the engine cycle. This adds other constraints on the nacelle length and trailing edge radius. Goulos [14] carried out Computational Fluid Dynamics (CFD) investigations of separate nozzle systems to derive the leading geometric terms and design guidelines for optimal shaping, successively building surrogate models for faster predictions [15]. The complex non-linear interaction between the design variables has been described by response surface models also in the case of the nacelle cowl [16], allowing for a cheaper scansion of the design space or a local refinement of the solution in a global search.

The present work reports a tool to carry out a design space exploration (DSE) for a UHBPR nacelle with two approaches featuring a different level of complexity and accuracy. In view of the quite large number of decision variables that can be used to represent the set of nacelle curves and their interaction, the identification of the feasible regions of the design space is more effectively achieved by a global optimisation search, that generates a dataset that can be used lately for a local refinement or a surrogate model training. Genetic optimisation algorithms (GA) are suitable to this task, as they can naturally cope with the multi-objective constrained nature of the problem and obtain Pareto optimal solutions. However, this typically requires a large number of CFD evaluations that makes the research time-expensive. In this work, a first tool based on a leaner computational model and a standard GA is used to rapidly obtain indications on the main trends and guide the research towards feasible and optimal regions of the design space. A second tool based on a more accurate computational model and a more advanced optimisation algorithm is employed, starting from the previous results, to complete the analysis. The investigated nacelle shapes target a long haul civil application, and they are meant to be installed on the NASA Common Research Model (CRM) aircraft body in future studies, in the framework of the EU Clean Sky 2 project IVANHOE.

III. Methods

A. Geometric parameterisation

The preliminary sizing of the nacelle overall dimensions was derived from the inputs of a turbofan thermodynamic cycle design, assuming state of the art technologies and ultra-high bypass ratio. Figure 1 shows the geometric parameters controlling the nacelle, among which the highlight radius R_{HL}, the nacelle length L_{nac}, the trailing edge radius R_{TE} determine the overall size, whilst the ratios R_{max}/R_{HL}, L_{max}/R_{HL}, and the angle β_{TE} greatly influence the drag characteristics and can be optimised, together with additional variables locally controlling each curve shape. Other ratios used in the text are the lip nose radius factor f_{nose} and $f_{max} = L_{max}/R_{hl}$. Baseline values of the parameters were determined from indications reported in the open literature and constraints related to the specific engine design. In

particular, R_{HL} is associated to the engine mass flow and the fan diameter, L_{nac} is bound by the turbofan architecture and the tolerance to off-design conditions, R_{TE} and the slope angle β_{TE} influence the isentropic Mach number distribution on the external cowl and must also fit with the required bypass nozzle area and shape. The precise curve shape could be controlled thanks to an-house fully parametric tool, allowing to represent each curve describing the engine cross section, including the intake duct, the spinner and the exhaust system, with Bézier, B-Splines or Non-uniform Rational B-Splines (NURBS), choosing the number of control points, curve degree, knots positions and weight to reconstruct the geometry. The geometric modelling tool interfacing with the optimisation schemes allowed to have a fine local control of each curve and change the nacelle global dimensions at the same time. The tool also makes possible to introduce an arbitrary three-dimensional contouring using a smooth azimuthal distribution to connect the crown and keel profiles and account for scarf and droop.

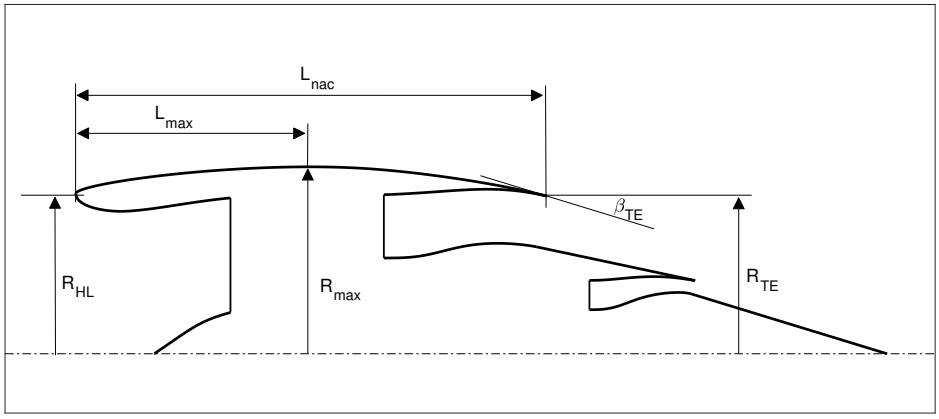

Fig. 1 Global nacelle dimensions.

B. Performance metrics

The performance metric considered in the study was the nacelle drag in different conditions. It is determined by three main force contributions, that act on the captured and ejected streamtube [17]:

$$D_{nac} = \phi_{pre} + \phi_{nac} + \phi_{post} \tag{1}$$

where ϕ_{pre} is the force integral on the pre-entry streamtube, ϕ_{nac} is the force integral on the nacelle external cowl, from the stagnation point on the fore lip to the trailing edge, ϕ_{post} is the post-exit force acting on the ejected streamtube. For the calculation of these three terms, the modified near-field approach of Christie [18] was used for the first, whilst direct surface integration was employed for the others. The nacelle operation was characterised by its mass flow capture ratio (MFCR), defined as the ratio between the far-upstream cross-sectional area of the captured streamtube A_0 and the highlight area $A_{hl} = \pi\, r_{hl}^2$, $MFCR = A_0/A_{hl}$. A typical value around 0.75 was chosen at cruise. The drag normalisation at different operating points defines the following drag coefficients considered in the study:

$$C_{d,cruise} = (D_{nac}@cruise) \,/\left(0.5\rho_\infty v_\infty^2 A_{hl}\right) \tag{2}$$

$$C_{d,spillage} = (D_{nac}@MFCR = 0.8cruise) \,/\left(0.5\rho_\infty v_\infty^2 A_{hl}\right) \tag{3}$$

$$C_{d,DD} = (D_{nac}@M = M_{cruise} + 0.02) \,/\left(0.5\rho_\infty v_\infty^2 A_{hl}\right) \tag{4}$$

The first component in eq. 2 refers to the nacelle cruise drag. The reference cruise condition was set at $M = 0.85$ at an altitude of 10667 m as from NASA CRM design point. The second metric of eq. 3 is the spillage drag, defined as the drag increment from cruise to end of climb, where MFCR is assumed to decrease to 80% of the initial value. The last component in eq. 4 is the Mach drag divergence, which measures the sensitivity of drag coefficient to change in flight Mach number, $\partial C_d/\partial M$, and it is usually calculated by finite difference with a 0.02 ΔM [12].

C. Computational method

The evaluation of the performance metrics involved in the optimisation problems was carried out using a CFD tool solving 2D axisymmetric Reynolds-Averaged Navier-Stokes (RANS) equations on different grids. The $\kappa - \omega$ SST turbulence model was employed with $y^+ < 1$ on the walls, to resolve the boundary layer and the shock-wave interaction occurring on the curved cowl. The points were distributed based on meshing guidelines from literature and a grid sensitivity study on performance metrics. The validation of the computational model for drag prediction was carried out using experimental data from axisymmetric nacelle cowls tests at ARA [19]. A structured multi-block grid with three levels, coarse (C), medium (M), and fine (F) having a refinement factor of $\sqrt{2}$ starting from 25k elements was employed in the sensitivity analysis. The grid convergence was measured by the grid convergence index (GCI) [20] computed on the nacelle drag. In the test case, different nacelle cowls were tested in wind tunnel experiments to measure their drag. The Cowl 1 type is here considered. The nacelle featured a cylindrical centerbody and was supported by a cylindrical sting attached to a conical support. The drag was measured by wake integration of momentum deficit with a plane rake located 0.169 L_{nac} downstream of the leading edge, on the sting, and therefore it included a small contribution from the support that was equally considered in the CFD. Figure 2 reports the variation of the nacelle drag coefficient with the MFCR at $M = 0.85$ and the sensitivity to the Mach number at $MFCR = 0.60$. The grid convergence analysis gave an average apparent order of convergence of 2.1725 with a GCI^{21} always inferior to 1%, suggesting that a medium mesh level was sufficient to capture the drag coefficient and its sensitivity to spillage and drag divergence.

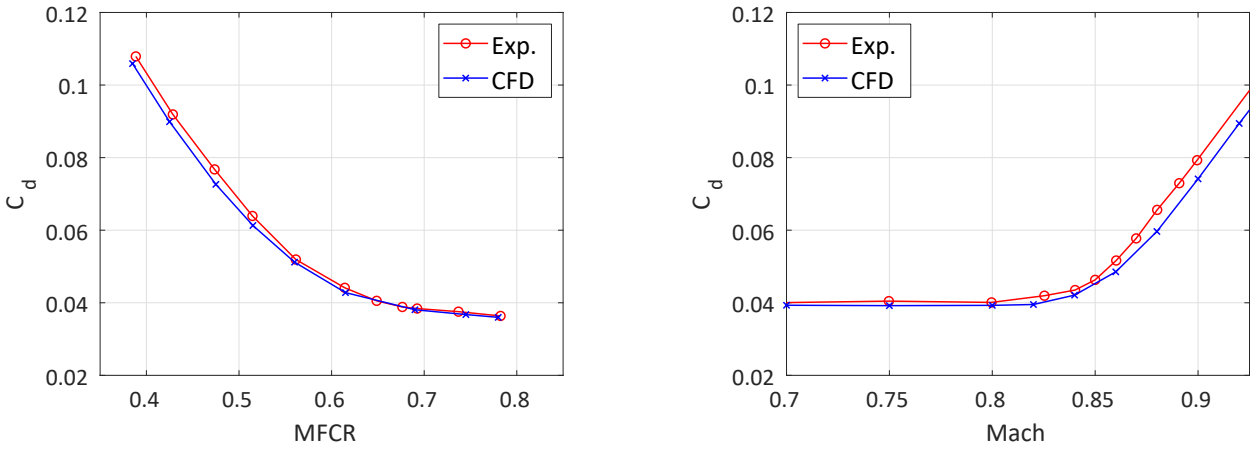

(a) Cd vs MFCR at M=0.85 **(b) Cd vs Mach at MFCR=0.60**

Fig. 2 Sensitivity of nacelle drag to MFCR and Mach number for ARA Cowl 1 in experimental and CFD tests.

The point distribution validated for the ARA cowl was reused in the grids employed for the design space exploration. In the initial coarser exploration, in order to reduce the computational time and the cost of the deployment of an automatic body-fitted multi-block mesh generation for a generic nacelle shape, an hybrid meshing strategy was adopted. The boundary layer was meshed using a structured wall-resolved O-grid that was grown until an isotropic mesh layer was obtained. The outer part of the domain was filled with an unstructured distribution up to the semicircular farfield boundary located $60R_{max}$ far. The exhaust region was refined in order to capture the jet expansion with sufficient accuracy. For the finer exploration, a structured multi-block grid was employed, granting higher accuracy in predicting the absolute drag coefficients and their sensitivity to freestream conditions and also the jet expansion and interaction between the bypass and core streams. The number of cells was 100k in this case, compared to 30k in the hybrid approach, with a computational cost proportional to the size ratio. An example of this mesh is shown in Figure 3.

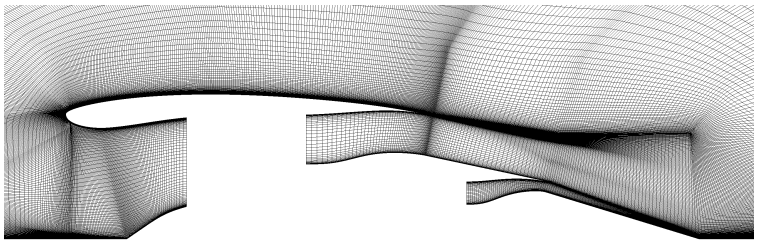

Fig. 3 Example of structured multi-block mesh used in the second refined optimisation.

Table 1 Initial DSE parameters and ranges

Parameter	Range
L_{nac}/R_{hl}	2.45-3.5
R_{max}/R_{hl}	1.09-1.26
L_{max}/R_{hl}	0.28-0.48
R_{te}/R_{hl}	0.87-1.01

IV. Design Space Exploration

A. Initial DSE

The first design space exploration was based on the leaner computational model. The investigation aimed to solve the three-objective multi-point optimisation problem:

$$minimise \begin{cases} C_{d,cruise} \\ C_{d,spillage} \\ C_{d,dd} \end{cases} \tag{5}$$

in order to find the most promising region of the design space, corresponding to favourable geometric ratios of the nacelle.

Before focusing on the derivation of most promising nacelle shapes, the global dimensions of the nacelle were investigated in a Design of Experiment (DOE), in order to reduce their ranges and help the optimisation algorithm to reach the Pareto frontier. These global dimensions determine the overall size and have a strong effect on the flow field and drag figures. The initial ranges of variation were selected based on open literature information and are listed in Table 1. The four design variables are expressed in terms of geometric ratios: L_{nac}/R_{hl}, R_{max}/R_{hl}, L_{max}/R_{hl}, and R_{te}/R_{hl}.

Figure 4 shows the projected three-dimensional scatter plot of the population of 150 individuals generated through a Latin Hypercube sampling. It can be seen that the $C_{d,cruise}$ and $C_{d,dd}$ were found to be not conflicting, whilst a Pareto front emerged for the $C_{d,cruise}$-$C_{d,spillage}$ projection. Also visible is the fact that higher isentropic Mach number peaks were not necessarily associated to the largest drag coefficients, although from a practical standpoint configurations with $M_{iso} > 1.3$ are to be discarded, as once installed the wing upwash and the gulley formed within the wing-nacelle-pylon will further increase the peak on the upper lip, and also off-design performance and high-incidence operation can be degraded. It must be considered, in addition, that being varied only four global dimensions at that stage, a fine control on the maximum Mach number, occurring close to the leading edge, could not be obtained, whereas in the subsequent optimisations where the curves were fully parameterised the constraint were more accurately fulfilled.

The relation between the main dimensions and the objectives is highlighted in Figure 5, where it can be noticed that not all the selected combinations gave rise to feasible designs. For example, too slim nacelles tend to produce an excessive acceleration, which was reduced by increasing the R_{max} at the expense of drag coefficient. Nacelles too short or with a short forebody had a more scattered drag distribution with values largely above the mean. The trailing edge radius was found to be less correlated, as it is thought to be dependent on the maximum height, determining the trailing edge angle and thus the pressure recovery on the rear portion of the cowl and the position of the strong shockwave. An analysis of the isentropic Mach number distribution at cruise revealed the presence of three main patterns: a high suction peak terminated with a strong front shock for a long nacelle; a lower peak with a shock wave occurring closer to

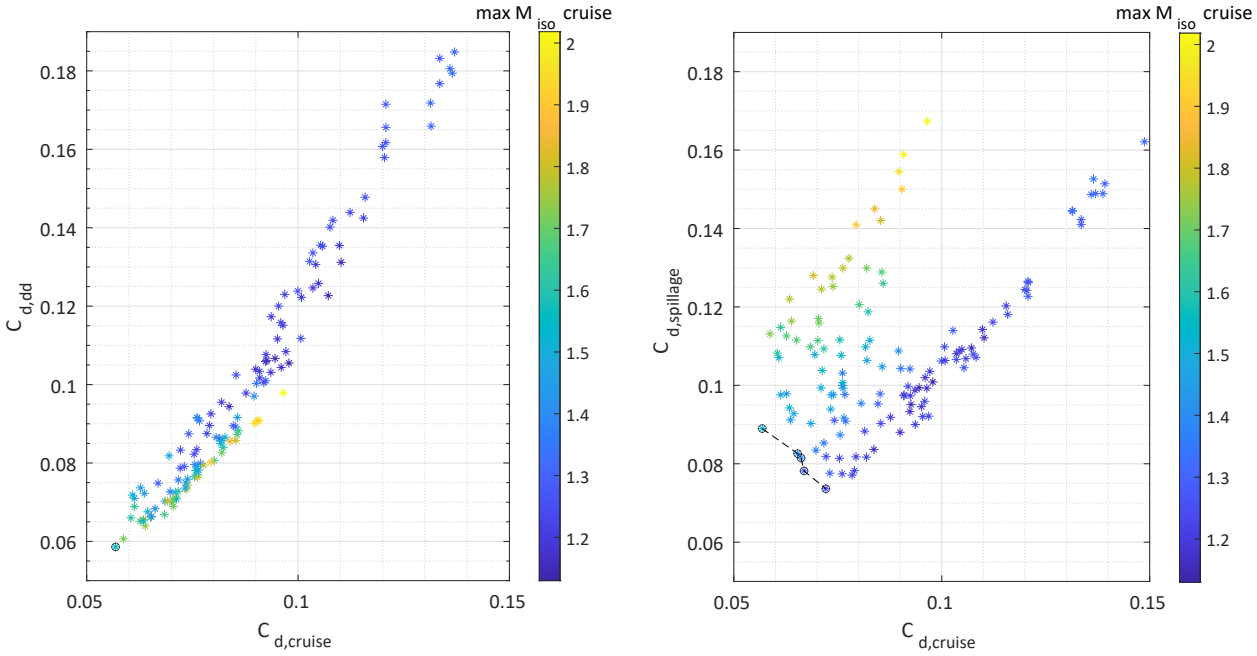

Fig. 4 Projected Pareto frontier for initial global size exploration.

maximum radius, preceded by a modest reacceleration; an intermediate peak with a double shock in the first half of the cowl. An accurate control on this distribution is necessary to obtain a balanced behaviour at cruise and off-design operation and Figure 5 highlights a clear correlation between the peak value and the ratio R_{max}/R_{hl}.

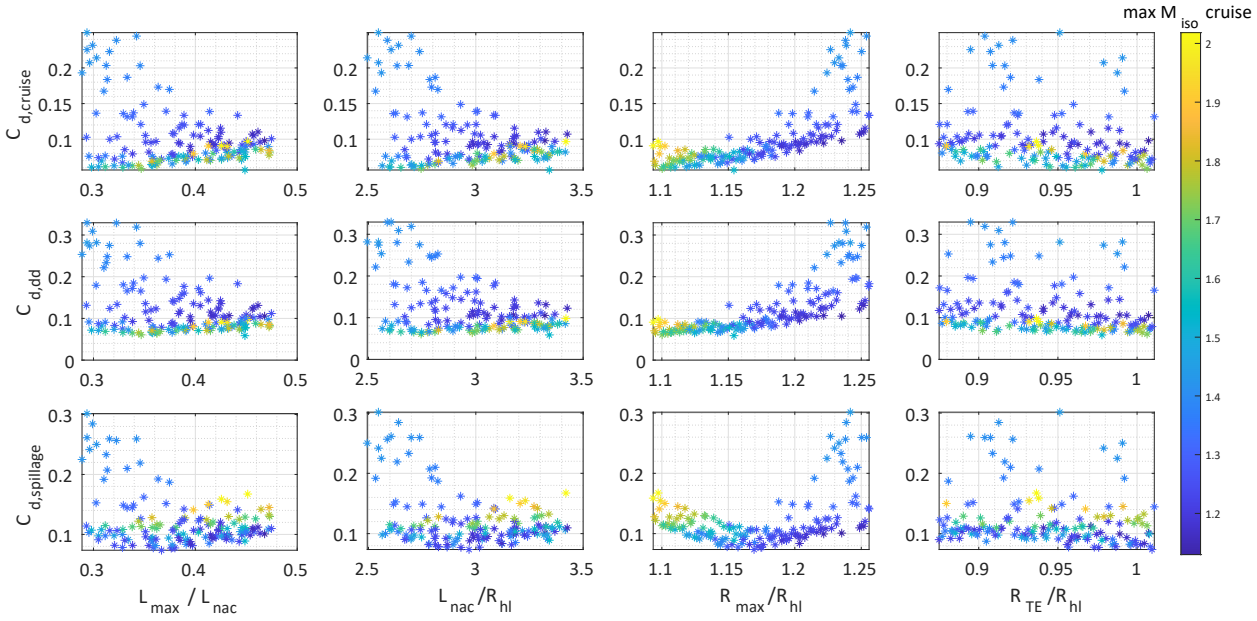

Fig. 5 Dependence of performance metrics on design variables for initial DSE.

The outcome of the DOE for suitable global ratios allowed to refine the searching bounds of these dimensions and focus in more promising regions of the design space in a first optimisation-driven DSE for optimal Pareto solutions searched with the NSGA-II algorithm [21]. The number of design variables was eight and they controlled the local external cowl shape. The optimisation was terminated after 20 generations with a population size of 30 individuals. The

finally reached Pareto frontier is shown in Figure 6. The reported maximum isentropic Mach number ranges from 1.3 to 1.35. Its tendency was to be positively correlated to the spillage drag, and negatively to the cruise drag.

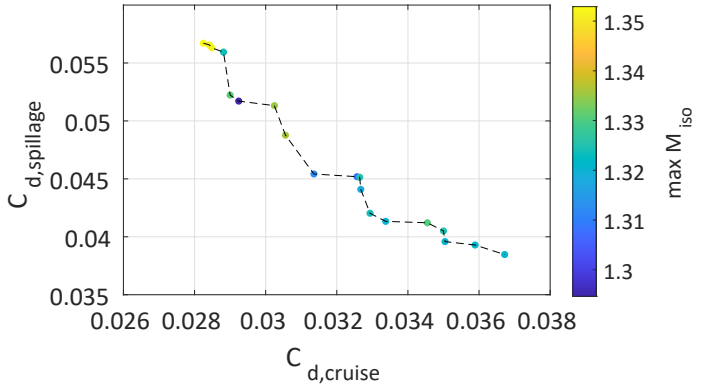

Fig. 6 Pareto Frontier for the first DSE.

Examples of its distribution on selected Pareto points are depicted in Figure 7, where it can be observed that in cruise condition the best cruise sample had a smooth deceleration up to 40% of chord, whilst the others presented a double-shock pattern.

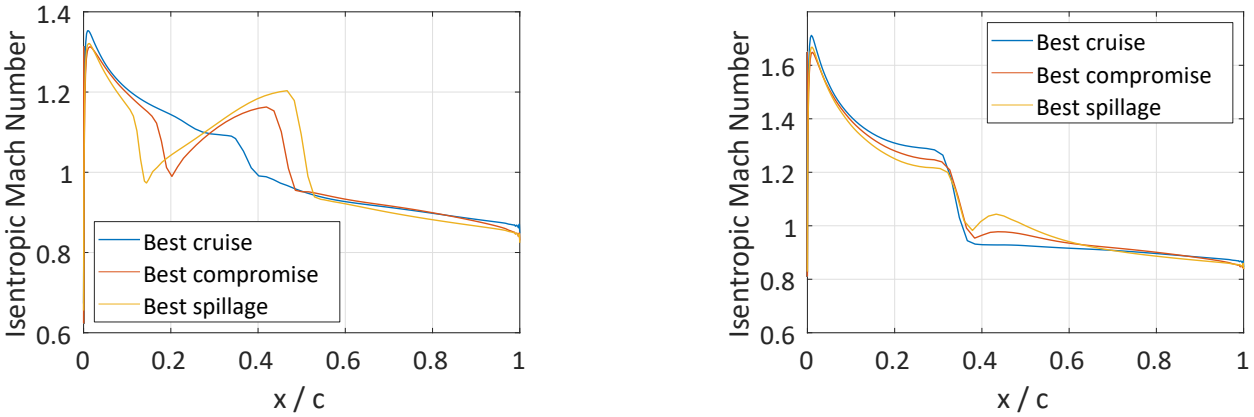

(a) Cruise condition

(b) Spillage condition

Fig. 7 Mach number distribution on the external cowl for selected Pareto solutions of the initial DSE.

B. Refined DSE

Based on the indications of the initial DSE in terms of likely positioning of optimal solutions and more suitable geometric ratios, a subsequent optimisation problem based on higher-accuracy tools was solved. A more advanced GA was employed, the GeDEA-II algorithm, relying on unique genetic operators driving the research towards the Pareto frontier by explicitly including genetic diversity as a real objective [22–24]. The optimisation problem was formulated as:

$$minimise \begin{cases} C_{d,cruise} \\ C_{d,spillage} \end{cases} \tag{6}$$

with $maxM_{iso}$@cruise < 1.30

The drag divergence was not explicitly put as an objective, given the lower sensitivity resulting from the previous investigation. Instead, a constraint on the maximum isentropic Mach number was added to control the off-design performance and promote the generation of smoother deceleration profiles without excessive shocks at cruise, that will inevitably grow when operating in installed or off-design condition.

The number of design variables was ten, with nine of them related to the external cowl shape and one controlling the highlight radius. As highlighted above, its position is very relevant for the cruise drag and the off-design performance, and it is usually derived from the required engine mass flow in order to have a MFCR of 0.7-0.75 at cruise. Here the mass flow was kept fixed, being related to the required thrust. As the drag figures are sensitive to small variations of this parameter, it was allowed to slightly vary around the baseline point, so as the resulting MFCR was in the typical range and its position always fit with respect to the fan diameter. Like in the previous case, the trailing edge position was kept fixed, being dictated by the bypass nozzle requirements in terms of duct contouring, exit area and trailing edge thickness. Its staying unchanged was compensated by the freedom of the highlight point, allowing to vary according to the ratio R_{TE}/R_{HL}.

The optimisation was terminated after 20 generations with a population size of 30 individuals. The total computational time was 114 hr for 540 CFD calls. The finally reached Pareto frontier is shown in Figure 8. The analysis of the front reveals that its extent was larger in the second objective, and the spillage difference became almost zero in the rightmost points. The C_d at drag divergence, reported with the colour scale in the figure, was confirmed to be almost proportional to the one in cruise. The cowl corresponding to the best cruise had a slightly higher highlight radius but a lower thickness, compared to the best compromise and best spillage drag. These two were equally slimmer, but with a lower highlight radius. The trend towards a reduction of the highlight can be explained by the corresponding increase of the MFCR and decrease of the pre-entry drag during spillage condition. The generation of slimmer shapes can be similarly related to a lower cruise drag, but it must compete with a worse deceleration control at higher Mach. The higher density in the Pareto front compared to that of Figure 6 can be attributed to the use of a good initial population for this refined optimisation, but also to the superior capability of the GeDEA-II algorithm in finding the non-dominated solutions.

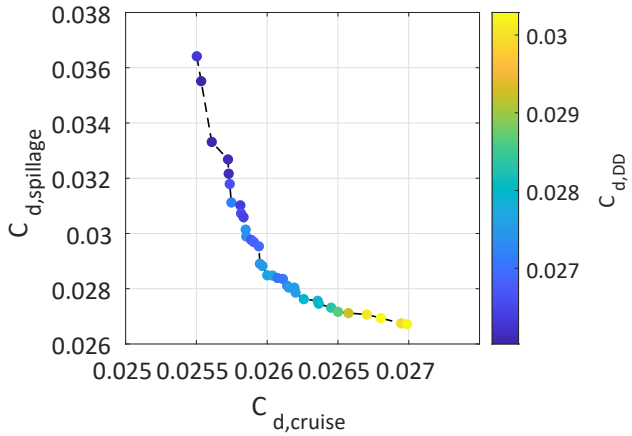

Fig. 8 Pareto front for the second optimisation problem.

The relationship between the geometric parameters and the objectives is reported in the scatter plots of Figures 9 and 10. The first one shows the correlation with the cruise drag. The highlight radius is measured by the equivalent MFCR, from which it can be noticed that the minimum falls around 0.735, but many Pareto points, plotted in blue, are close to the upper bound. This will be explained later, when examining the tendency of the spillage drag. In terms of location of maximum thickness, best values were found within 0.36 and 0.42, with a weak decreasing trend of C_d towards the lower bound. The optimal maximum thickness ratio was within 1.135 and 1.165, with slimmer shapes showing a small reduction of drag. Values of the local slope at the trailing edge were, instead, more constrained and probably not completely generalisable, but in the present case feasible geometries featured $\beta_{TE} \approx 13 - 14°$. The distribution of the nose radius had a parabolic-like shape, with the minimum C_d found at 0.03. Finally, regarding the trailing edge height it was found to have an optimal value minimising the cruise drag at around 0.98, but for the spillage condition it resulted to be constrained by the minimum achievable highlight radius. Actually, R_{hl} appeared to be more correlated to that off-design operation, as visible in Figure 10. The tendency of the optimiser, as highlighted before, was to reduce it and increase the MFCR consequently. A significant negative correlation coefficient can be observed in Figure 10 for the MFCR and, as it was directly proportional to, for the R_{TE}/R_{hl} ratio. A further reduction of the highlight radius was not tolerable, as this was dictated by the required mass flow rate, the fan radius, the need for a sufficiently high inlet contraction ratio without an excessive throat Mach number. It is interesting to notice a clearly conflicting requirement for the nacelle thickness, that is highly negatively correlated with the spillage drag.

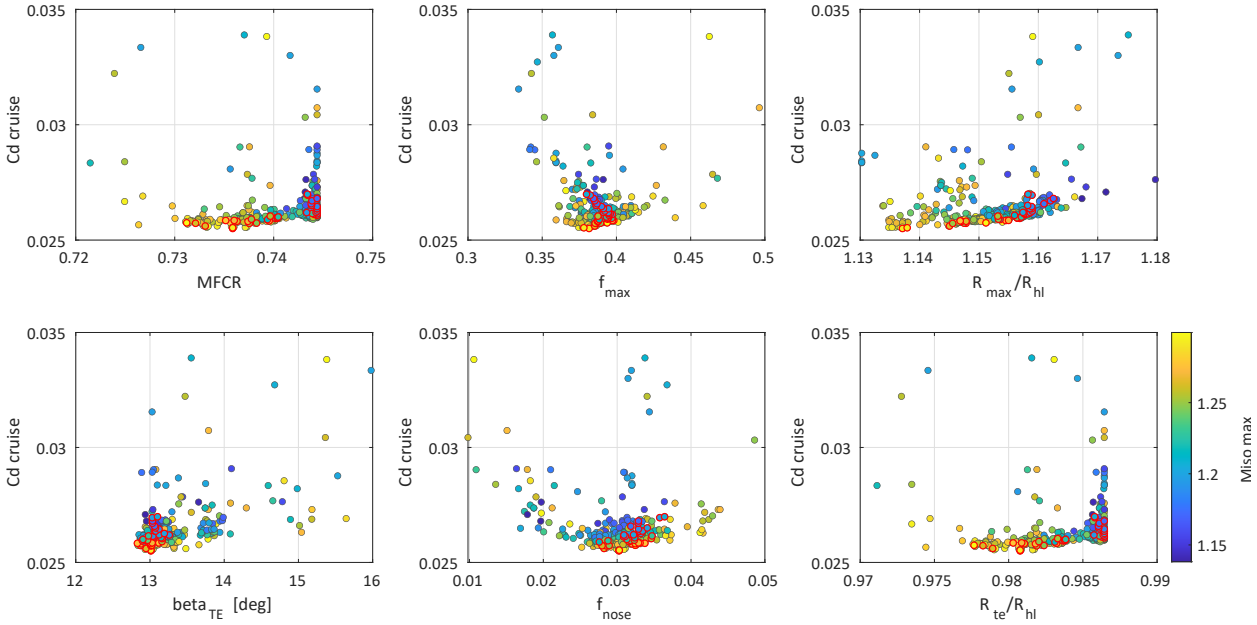

Fig. 9 Correlation of cruise drag coefficient with nacelle geometric ratios. Pareto points are circled in red.

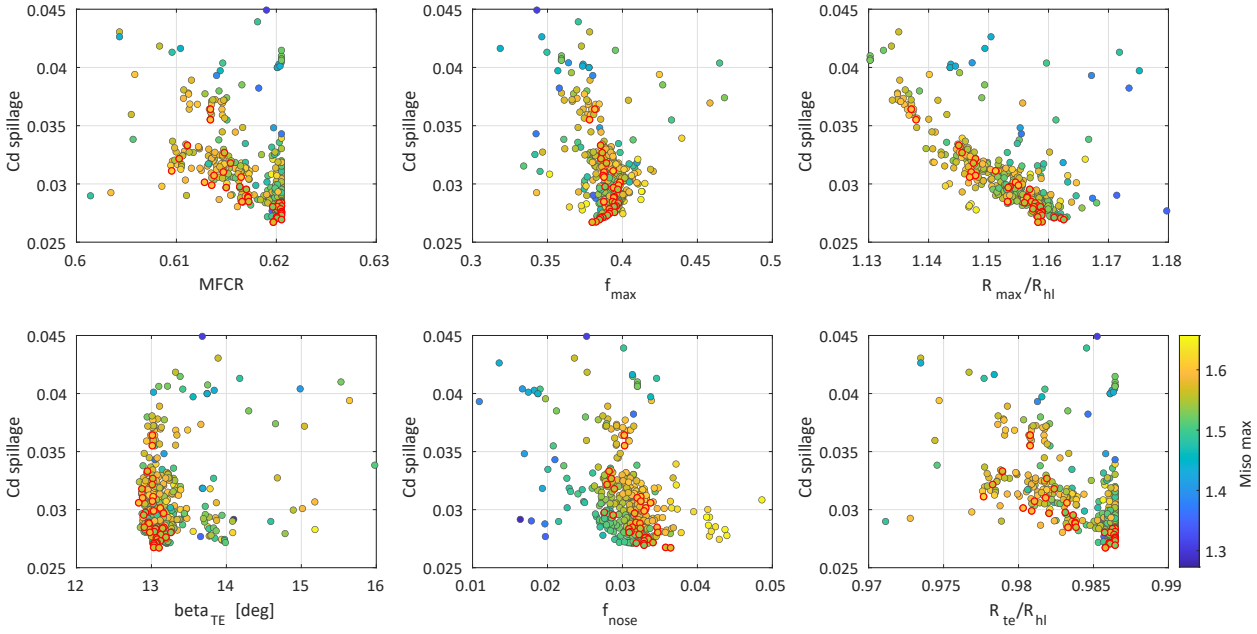

Fig. 10 Correlation of spillage drag coefficient with nacelle geometric ratios. Pareto points are circled in red.

The isentropic Mach number distribution for selected Pareto solutions is reported in Figure 11. On Figure 11a the cruise distribution appears to be almost shock-free for the best cruise nacelle, with a peak just below the threshold. The best compromise and best spillage have quite similar curves, with a more evident double shock pattern for the first; in that case, the leading edge shock is followed by a flow reacceleration that is terminated by another shock wave, at the same chordwise position of the best compromise cowl, just after the maximum thickness point. At reduced mass flow rate, Figure 11b, the best cruise nacelle had the largest maximum M_{iso} peak of 1.6, followed by a quite strong shock wave at 0.26 x/c. The other two nacelles had slightly lower values of peak Mach number, but whilst the best compromise presented a shock wave at 0.25 x/c followed by another expansion, the best spillage featured an almost

shock-free profile, like in the cruise condition of the best cruise cowl, which explains the better performance.

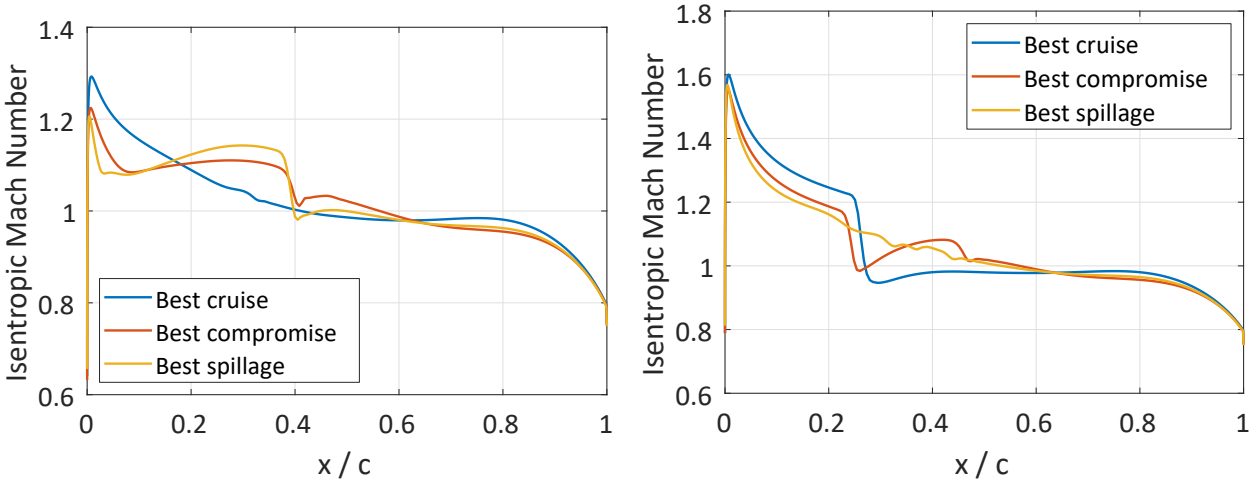

(a) Cruise condition **(b) Spillage condition**

Fig. 11 Mach number distribution on the external cowl for selected Pareto solutions.

The flow field for the selected Pareto sampled is shown in Figure 12. The absence of a strong shock wave for the best cruise individual can be appreciated, whereas in the other two samples the shock occurs near the maximum thickness. The nozzle shapes remained the same, instead, leading to an identical jet expansion.

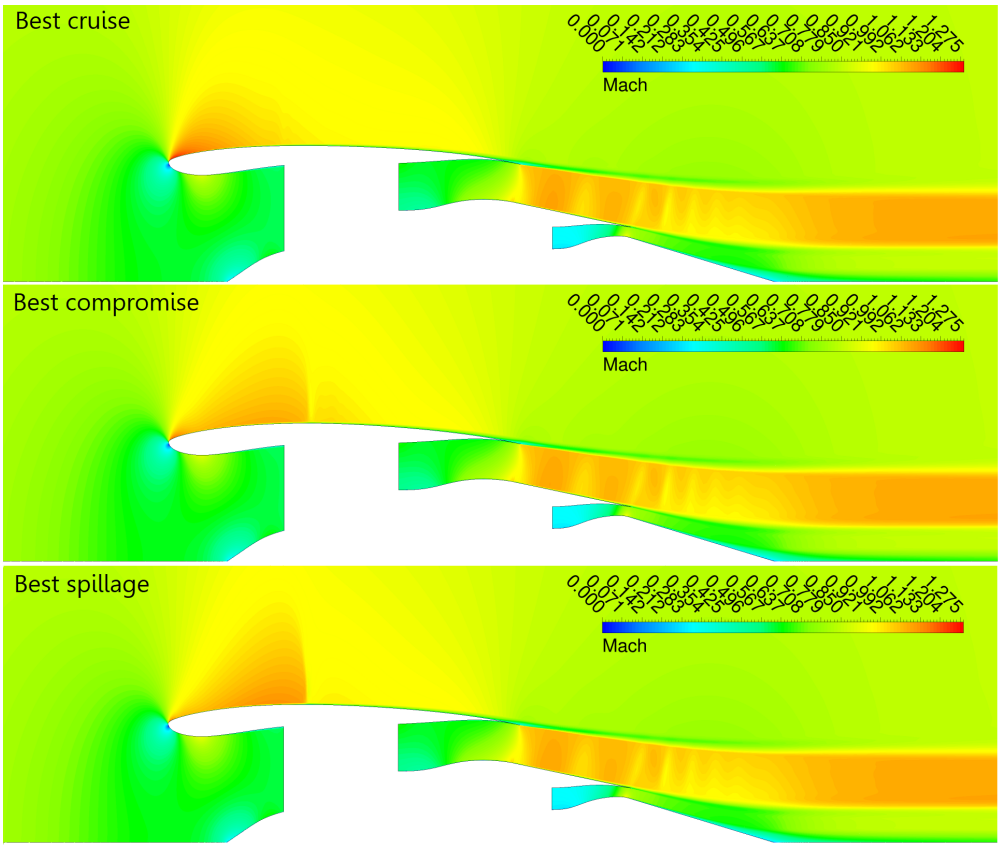

Fig. 12 Mach number distribution for selected Pareto individuals.

Comparing the results obtained with the set of refined tools to those reported in the previous section for the initial DSE, the accuracy of the leaner model can be established. As mentioned above, the purpose of using a less complex and faster numerical model was to loosely scan the design space and obtain information on suitable regions, geometric ratios and flow features of the best promising shapes. The correlations between the objectives and the relevant geometric parameters of Figure 5 were substantially confirmed in the second DSE. The isentropic Mach number distribution on Pareto points was also equally present in both the investigations, suggesting that smoother profiles are associated to lowest drag coefficients, but this is evidently conflicting as almost shock-free profiles at one condition always produce strong shocks at a different engine setting or flight speed. Best compromise solutions feature a single shock located near the maximum cowl thickness, with a partial reacceleration either upstream or downstream, depending on the point considered.

The variation found between the two CFD models was due primarily to a different computed post-exit force. As expected, given the fact that it was calculated from pressure integration on the ejected streamtube, the finer structured grid with better flow-aligned stretched cells produced a more accurate value of the ϕ_{post} component. In this study, the engine thrust settings and the exhaust system were the same in both the explorations, such that the difference in the absolute drag values of the leaner model was almost constant. The identification of the main trends and optimal features of the simpler tool was therefore confirmed also in the refined exploration.

V. Conclusion

A geometric parameterisation tool for the design of UHBPR turbofan nacelles has been developed. The influence of relevant global geometric dimensions on the drag coefficient of the nacelle has been first investigated in a design of experiment, serving as the basis for a first optimisation-driven design space exploration on drag coefficient at cruise and off-design conditions, based on a lean numerical tool with a cheap computational cost and development time. The useful indications coming from the investigation, in terms of optimal geometric ratios and flow features of most promising shapes have been used to run a second exploration with a more sophisticated tool. The good agreement between the two sets of results in terms of the relationship between the geometric parameters and the drag behaviour and the flow development over the external cowl for Pareto points show that the two-dimensional axisymmetric design of nacelle cowls can be oriented by using a multi-level approach with successive refinements for the design space exploration. The ranges derived in the study can provide important guidelines for future UHBPR nacelle design, and will form the basis for three-dimensional contouring of the external cowl and intake geometry. This shall be assessed as an additional degree of freedom to optimise both the external flow field and its interaction with the airframe and the coupling between the engine fan and the intake duct.

Acknowledgments

The authors wish to acknowledge the members of the IVANHOE consortium for the CleanSky 2 JU funded EU project, GA No. 863415 and in particular Chalmers University of Technology for the suggestions provided regarding the engine cycle study.

References

[1] European Commission, "FlightPath 2050," Tech. rep., ACARE, Luxembourg, 2011. https://doi.org/10.2777/50266, URL https://ec.europa.eu/transport/sites/transport/files/modes/air/doc/flightpath2050.pdf.

[2] Zimbrick, R. A., and Colehour, J. L., "Investigation of very high bypass ratio engines for subsonic transports," *Journal of Propulsion and Power*, Vol. 6, No. 4, 1990, pp. 490–496. https://doi.org/10.2514/3.25461.

[3] Berton, J. J., and Guynn, M., "Multi-Objective Optimization of Turbofan Design Parameters for an Advanced, Single-Aisle Transport," *AIAA*, , No. September, 2010, pp. 1–17. https://doi.org/10.2514/6.2010-9168, URL http://arc.aiaa.org/doi/10.2514/6.2010-9168http://www-psao.grc.nasa.gov/publications/AIAA-2010-9168.pdf.

[4] Bijewitz, J., Seitz, A., Hornung, M., and Luftfhart Bauhaus, E., "Architectural Comparison of Advanced Ultra-High Bypass Ratio Turbofans for Mesium to Long Range Application," *Deutscher Luft- und Raumfhahrtkongress 2014*, DLR, 2014, p. 12. URL http://www.dglr.de/publikationen/2015/340105.pdf.

[5] Kestner, B. K., Schutte, J. S., Gladin, J. C., and Mavris, D. N., "Ultra high bypass ratio engine sizing and cycle selection study for a subsonic commercial aircraft in the N+2 timeframe," *Proceedings of the ASME Turbo Expo*, Vol. 1, American Society of Mechanical Engineers (ASME), 2011, pp. 127–137. https://doi.org/10.1115/GT2011-45370.

[6] Magrini, A., Benini, E., Yao, H.-D., Postma, J., and Sheaf, C., "A review of installation effects of ultra-high bypass ratio engines," *Progress in Aerospace Sciences*, Vol. 119, 2020, p. 100680. https://doi.org/https://doi.org/10.1016/j.paerosci.2020.100680, URL http://www.sciencedirect.com/science/article/pii/S0376042120300920.

[7] *Aerodynamic Design Optimization of Nacelle and Intake*, Turbo Expo: Power for Land, Sea, and Air, Vol. Volume 2: Aircraft Engine; Coal, Biomass and Alternative Fuels; Cycle Innovations, 2013. https://doi.org/10.1115/GT2013-94857, URL https://doi.org/10.1115/GT2013-94857, v002T01A014.

[8] Savelyev, A., Zlenko, N., Matyash, E., Mikhaylov, S., and Shenkin, A., "Optimal design and installation of ultra high bypass ratio turbofan nacelle," *AIP Conference Proceedings*, Vol. 1770, No. 1, 2016, p. 030123. https://doi.org/10.1063/1.4964065, URL https://aip.scitation.org/doi/abs/10.1063/1.4964065.

[9] Fang, X., Zhang, Y., Li, S., and Chen, H., *Transonic Nacelle Aerodynamic Optimization Based on Hybrid Genetic Algorithm*, chapter and pages. https://doi.org/10.2514/6.2016-3833, URL https://arc.aiaa.org/doi/abs/10.2514/6.2016-3833.

[10] Christie, R., Heidebrecht, A., and MacManus, D., "An Automated Approach to Nacelle Parameterization Using Intuitive Class Shape Transformation Curves," *Journal of Engineering for Gas Turbines and Power*, Vol. 139, No. 6, 2017. https://doi.org/10.1115/1.4035283, URL https://doi.org/10.1115/1.4035283, 062601.

[11] Christie, R., Robinson, M., Tejero, F., and MacManus, D. G., "The use of hybrid intuitive class shape transformation curves in aerodynamic design," *Aerospace Science and Technology*, Vol. 95, 2019, p. 105473. https://doi.org/https://doi.org/10.1016/j.ast.2019.105473, URL http://www.sciencedirect.com/science/article/pii/S1270963819305450.

[12] Robinson, M., Macmanus, D. G., Richards, K., and Sheaf, C., "Short and slim nacelle design for ultra-high BPR engines," *AIAA SciTech Forum - 55th AIAA Aerospace Sciences Meeting*, American Institute of Aeronautics and Astronautics Inc., 2017. https://doi.org/10.2514/6.2017-0707.

[13] Tejero, F., Robinson, M., MacManus, D. G., and Sheaf, C., "Multi-objective optimisation of short nacelles for high bypass ratio engines," *Aerospace Science and Technology*, Vol. 91, 2019, pp. 410 – 421. https://doi.org/https://doi.org/10.1016/j.ast.2019.02.014, URL http://www.sciencedirect.com/science/article/pii/S1270963818315724.

[14] Goulos, I., Otter, J., Stankowski, T., MacManus, D., Grech, N., and Sheaf, C., "Aerodynamic Design of Separate-Jet Exhausts for Future Civil Aero-engines - Part II: Design Space Exploration, Surrogate Modeling, and Optimization," *Journal of Engineering for Gas Turbines and Power*, Vol. 138, No. 8, 2016. https://doi.org/10.1115/1.4032652.

[15] Giangaspero, G., MacManus, D., and Goulos, I., "Surrogate models for the prediction of the aerodynamic performance of exhaust systems," *Aerospace Science and Technology*, Vol. 92, 2019, pp. 77 – 90. https://doi.org/https://doi.org/10.1016/j.ast.2019.05.027, URL http://www.sciencedirect.com/science/article/pii/S1270963818328438.

[16] Heidebrecht, A., and MacManus, D. G., "Surrogate model of complex non-linear data for preliminary nacelle design," *Aerospace Science and Technology*, Vol. 84, 2019, pp. 399 – 411. https://doi.org/https://doi.org/10.1016/j.ast.2018.08.020, URL http://www.sciencedirect.com/science/article/pii/S1270963818303328.

[17] MIDAP Study group, "Guide to in-Flight Thrust Measurement of Turbo- jets and Fan Engines. Agardograph No. 237, Technical Report No. AG-237," Tech. rep., AGARD, London, 1979.

[18] Christie, R., "Propulsion System Integration and Modelling Synthesis," Phd thesis, University of Cranfield, 2016.

[19] Langley, M. J., "The design of axisymmetric cowls for podded nacelles for high by-pass ratio turbofan engines," Report and memoranda 3846, Aircraft Research Association Ltd., 1979.

[20] ASME, "Procedure for Estimation and Reporting of Uncertainty Due to Discretization in CFD Applications," *Journal of Fluids Engineering*, Vol. 130, No. 7, 2008. https://doi.org/10.1115/1.2960953, URL https://doi.org/10.1115/1.2960953, 078001.

[21] Deb, K., Pratap, A., Agarwal, S., and Meyarivan, T., "A fast and elitist multiobjective genetic algorithm: NSGA-II," *IEEE Transactions on Evolutionary Computation*, Vol. 6, No. 2, 2002, pp. 182–197. https://doi.org/10.1109/4235.996017.

[22] Ronco, C. C. D., and Benini, E., "GeDEA-II : A Novel Evolutionary Algorithm for Multi-Objective Optimization Problems Based on the Simplex Crossover and The Shrink Mutation," 2012.

[23] Comis Da Ronco, C., and Benini, E., "GeDEA-II: A Simplex-Crossover Based Multi Objective Evolutionary Algorithm Including the Genetic Diversity Asobjective," *Proceedings of the 14th Annual Conference Companion on Genetic and Evolutionary Computation*, Association for Computing Machinery, New York, NY, USA, 2012, p. 619–620. https://doi.org/10.1145/2330784.2330888, URL https://doi.org/10.1145/2330784.2330888.

[24] Benini, E., Venturelli, G., and Łaniewski Wołłk, ., "Comparison between pure and surrogate assisted evolutionary algorithms for multiobjective optimization," *Frontiers in Artificial Intelligence and Applications*, Vol. 281, 2016, pp. 229–242. https://doi.org/10.3233/978-1-61499-619-4-229, URL https://www.scopus.com/inward/record.uri?eid=2-s2.0-84964684002&doi=10.3233%2f978-1-61499-619-4-229&partnerID=40&md5=2f76419a488cc5e0e14dec05ba848180.